Spectrochimica Acta Part A: Molecular and Biomolecular Spectroscopy 272 (2022) 121003

Contents lists available at ScienceDirect

Spectrochimica Acta Part A: Molecular and Biomolecular Spectroscopy

journal homepage: www.elsevier.com/locate/saa

A universal sensing platform based on iron and nitrogen co-doped carbon dots for detecting hydrogen peroxide and related metabolites in human fluid by ratiometric fluorometry and colorimetry

Wei Zhang [a], Yanhua Wu [b], Xin Liu [a], Yibing Liu [a], Yue Zhang [a], Wei Wang [a], Xiaowei Mu [a], Rui Su [a], Ying Sun [a], Daqian Song [a], Xinghua Wang [a,*]

[a] College of Chemistry, Jilin University, Qianjin Street 2699, Changchun 130012, China
[b] Division of Clinical Research, The First Hospital of Jilin University, Changchun 130021, China

HIGHLIGHTS

- A sensing platform based on Fe/N-CDs and o-phenylenediamine (OPD) was developed for determination of xanthine and uric acid in real human fluid samples.
- Both the fluorescent property and the peroxidase-like property of Fe/N-CDs facilitate the improvement of analytical performance of the developed sensing platform.
- Ratiometric fluorescent and colorimetric testing modes endow the sensing platform with both high sensitivity for quantitative analysis and facile observation for qualitative analysis.

GRAPHICAL ABSTRACT

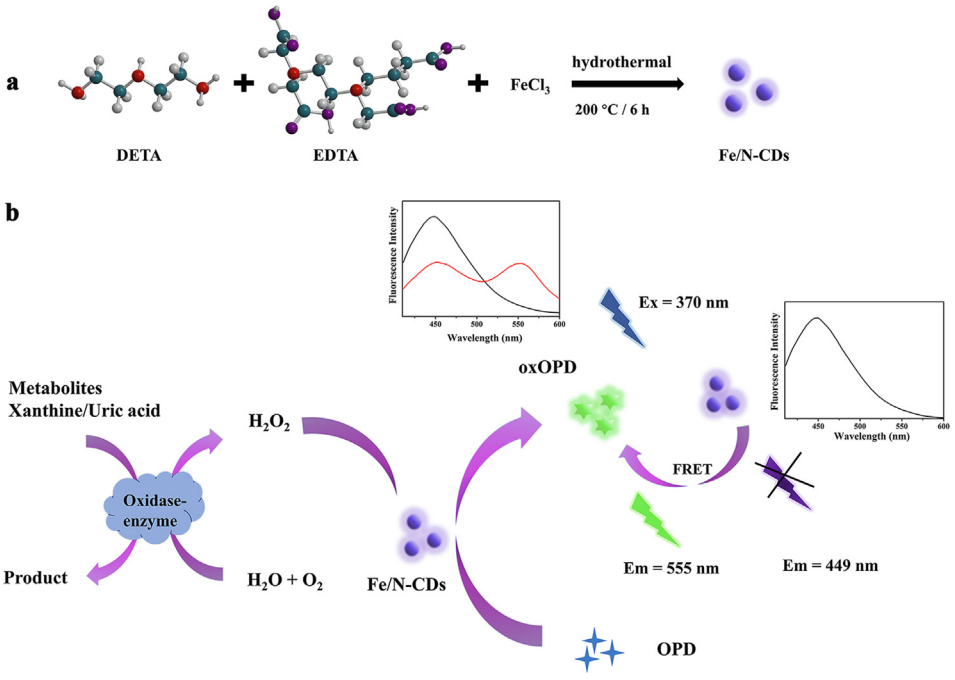

ARTICLE INFO

Article history:
Received 5 December 2021
Received in revised form 29 January 2022
Accepted 1 February 2022
Available online 5 February 2022

Keywords:

ABSTRACT

A universal ratiometric fluorescence and colorimetric dual-mode sensing platform for detecting hydrogen peroxide (H_2O_2) and related metabolites in human fluid was constructed based on iron and nitrogen co-doped carbon dots (Fe/N-CDs). As a fluorescent nanomaterial with peroxidase-like property, Fe/N-CDs emits fluorescence at 449 nm (F_{449}) under excitation of incident ultraviolet light, and can catalyze the oxidation of o-phenylenediamine (OPD) by H_2O_2 for generating 2,3-diaminophenazine (oxOPD) that exhibits obvious absorption at 420 nm (A_{420}) and fluorescence emission at 555 nm (F_{555}). The Förster resonance energy transfer (FRET) between Fe/N-CDs and oxOPD would result in the fluorescence quenching Fe/N-

* Corresponding author.
E-mail address: wxhchem@jlu.edu.cn (X. Wang).

https://doi.org/10.1016/j.saa.2022.121003

Iron and nitrogen co-doped carbon dots
Ratiometric fluorometry
Colorimetry
H_2O_2
Human fluid

CDs and the fluorescence enhancement of oxOPD, which facilitates the quantitation of oxOPD by ratiometric fluorometry. Since the amount of generated oxOPD is determined by the amount of H_2O_2 consumed during the oxidation reaction, the detection of H_2O_2 and related metabolites can be realized by monitoring both ratiometric fluorescent (F_{555}/F_{449}) and colorimetric (absorption, A_{420}) signals of oxOPD. This dual-mode sensing platform exhibits excellent selectivity and sensitivity toward with H_2O_2, xanthine and uric acid in both human serum and urine samples, demonstrating its good potential for monitoring H_2O_2 and metabolites involved in H_2O_2 metabolism in human body. The detection limits (LODs) of H_2O_2, xanthine and uric acid obtained by this sensing platform were 0.07, 0.15, and 0.14 μM for ratiometric fluorescence mode, and 0.12, 0.52, and 0.47 μM for colorimetric mode, respectively. By utilizing appropriate oxidases in this universal sensing platform, the determination of other metabolites involved with producing H_2O_2 can also be realized facilely.

1. Introduction

Hydrogen peroxide (H_2O_2) as one type of reactive oxygen species in human body is an inevitable byproduct of cell metabolism and serves as a signaling molecule for indicating physiological activities or oxidative stress [1]. Moreover, a large variety of metabolites in human body such as cholesterol, xanthine, glucose, lactate, choline, glutamate and alcohol can be oxidized to produce H_2O_2 under the catalysis of corresponding enzymes [2]. Xanthine is an intermediate generated in the metabolism of animal purine nucleotides and deoxynucleotides. Normal xanthine concentration ranges in body fluids of healthy human are 0.5–2.5 μM for plasma and 40–160 μM for urine [3]. And abnormal levels of xanthine in human fluids can indicate diseases including gout, uric acid deposits and renal calculus [4]. Uric acid is the final products of purine metabolism in human body [5]. Generally, the normal concentration ranges of uric acid are 0.13–0.46 mM in serum and 1.49–4.46 mM in urinary excretion [6]. Aberrant levels of uric acid in human fluid are related to gout, hyperuricemia, hypertension, urolithiasis, arthritis, cardiovascular and kidney diseases [7,8]. Since H_2O_2, xanthine and uric acid are essential biomarkers for clinical diagnosis, it is meaningful to develop efficient methods for sensitive and rapid detection of them in human fluid samples.

Nowadays, various analytical methods such as high-performance liquid chromatography (HPLC) [9], chemiluminescence [10], electrochemistry [11], colorimetry [12] and fluorometry [13] have been developed for quantitatively monitoring H_2O_2, xanthine and uric acid in biosamples. In most of these methods, enzymatic system usually plays key role for improving both sensitivity and selectivity due to the high specific and catalytic efficiency of enzymes [14]. Recently, more attention was focused on the nanomaterial-based artificial enzymes (nanozymes). Compared with natural enzymes, nanozymes display conspicuous features including high chemical stability, simple preparation and storage needs, good biocompatibility and tunable catalytic activity [15–17].

Fluorescent carbon dots (CDs) have been widely applied in chemical analysis, bioimaging and biosensing [18–20]. As is well known, heteroatom doping for CDs is an effective way to improve the functions of CDs and broaden their applications. It has been observed that trace metallic impurities, especially trace iron impurities in nanoparticles play very important roles for the peroxidase-mimicking activities of the nanoparticles [21,22]. Therefore, many types of Fe-doped CDs exhibit a comparable catalytic activity like natural peroxidases such as horseradish peroxidases (HRP) [23,24]. Compared with routine fluorometry based on the quenching or the enhancement of fluorescence at a single peak wavelength, the ratiometric fluorometry can effectively reduce the distractions of background and the fluctuations of instruments by employing the ratio of two fluorescence intensities at different peak wavelengths as a response signal, which not only makes the results more accurate but also improve the sensitivity greatly [25].

Herein, we synthesized a new type of iron and nitrogen co-doped carbon dots (Fe/N-CDs) (Scheme 1a) and employed it as both the fluorescent indicator and the catalyst for the oxidation reaction between o-phenylenediamine (OPD) and H_2O_2. By utilizing the absorption of the oxidative product 2,3-diaminophenazine (oxOPD) and the Förster resonance energy transfer (FRET) between Fe/N-CDs and oxOPD, a dual-mode sensing platform (Scheme 1b) with both ratiometric fluorescence and colorimetric readouts was constructed, of which the response signals were proportional to the amount of oxOPD generated during the oxidation reaction. Since the amount of H_2O_2 provided in a human fluid sample or originated from a H_2O_2 metabolism-involved metabolite determines the amount of oxOPD in the testing system, H_2O_2 or the corresponding metabolite can also be quantified by this sensing platform. Absorbance of the typical absorption band of oxOPD at 420 nm (A_{420}) and the intensity ratio of fluorescence emitted from oxOPD against that emitted from Fe/N-CDs (F_{555}/F_{449}) were employed as the ratiometric fluorescence and colorimetric response signals, respectively. Good accordance between the detecting results of xanthine and uric acid in real human fluid samples obtained by the developed sensing platform and the reference methods reveal the applicability of the developed sensing platform for future clinical diagnosis.

2. Experimental

2.1. Preparation of Fe/N-CDs

The Fe/N-CDs were synthesized according to a reported one-pot hydrothermal method with minor modification [26]. Briefly, 0.06 g of $FeCl_3{\cdot}6H_2O$, 0.10 g of EDTA and 0.06 mL of DETA were dissolved in 10 mL of ultrapure water. Subsequently, the mixture was transferred into a 30-mL Teflon-lined autoclaved, followed by heating at 200 °C for 6 h. The final product was diluted 2500-fold in PB buffer (10 mM, pH = 7.4) and was stored at 4 °C for further use.

2.2. Peroxidase-like activity and kinetic analysis of Fe/N-CDs

The peroxidase-like activity variation of Fe/N-CDs under different temperature and pH was investigated by carrying out the catalytic oxidation reaction of 3,3′,5,5′ -teramethylbenzidine (TMB). The relative catalytic activity (%) of Fe/N-CDs was defined as (A / A_{max} × 100%), in which A is the absorbance of a reaction system at 652 nm after incubating for 5 min, and A_{max} is the maximum value of A obtained by varying environmental temperature or pH.

The kinetic analysis of the catalytic reaction was performed by monitoring the absorbance at 652 nm of the reaction systems with various concentrations of TMB or H_2O_2. The dynamic parameters were calculated based on the Michaelis-Menten equation:

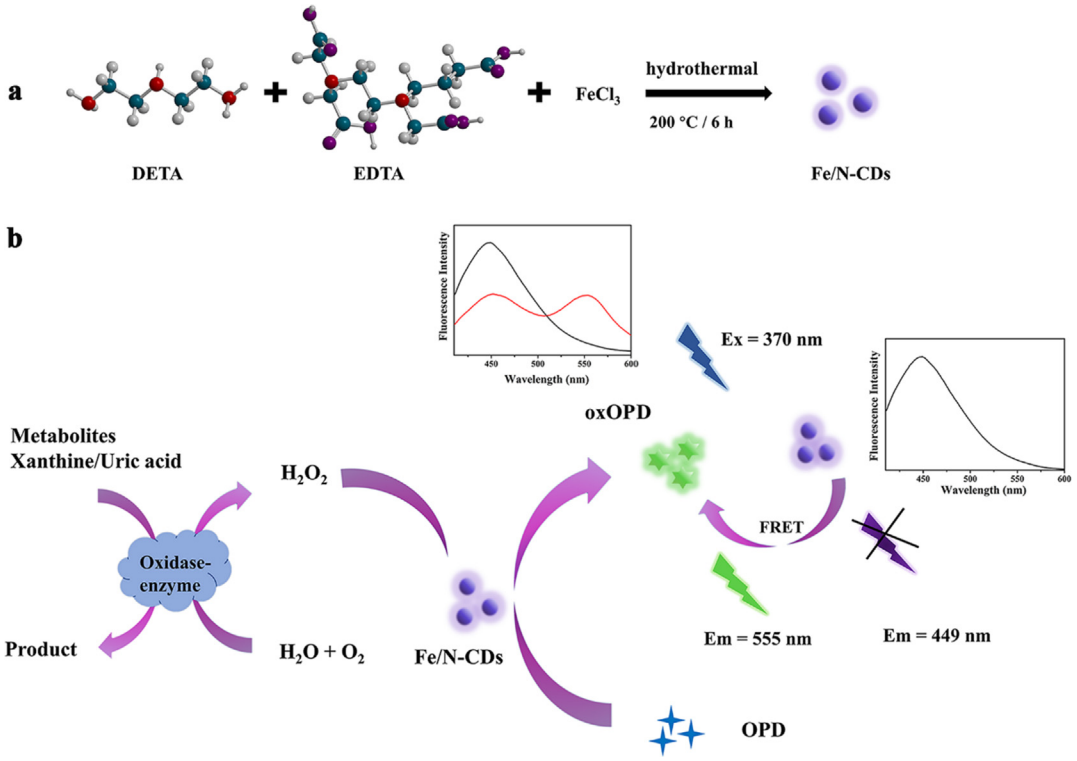

Scheme 1. Schematic diagram for detection of H_2O_2 and H_2O_2 metabolism-involved metabolites by the sensing platform developed in this work.

$$V_0 = \frac{V_{max} \times [S]}{K_m + [S]}$$

where V_0 and V_{max} respectively denote the initial and maximal velocities of the catalytic reaction, [S] and K_m respectively express substrate concentration and Michaelis constant. The velocities of each reaction were measured by monitoring the absorbance at 652 nm of the reaction system at 1.0 min interval.

2.3. Dual-mode detection of H_2O_2, xanthine and uric acid

To detect H_2O_2, 300 μL of OPD (10 mM), 40 μL of Fe/N-CDs, 100 μL of H_2O_2 solution at a certain concentration level were successively introduced into 560 μL of PB buffer (10 mM, pH = 7.4). The resulting solution was incubated at 37 °C for 30 min. Then the solution was examined by both ratiometric and colorimetric modes. Intensity ratio of fluorescence emission at 555 nm against that at 449 nm (F_{555}/F_{449}) at the excitation wavelength of 370 nm and absorbance at 420 nm (A_{420}) were respectively calculated or recorded as the response signals of the above detection modes.

To detect xanthine, 300 μL of OPD (10 mM), 40 μL of Fe/N-CDs, 50 μL of XOD (10 U/mL), and 100 μL of sample or standard solution containing xanthine were added into 510 μL of PB buffer (10 mM, pH = 7.4). The mixed solution was incubated for 30 min at 37 °C. The following procedures of incubation, spectral recording and data calculation are similar to these for detecting H_2O_2.

To detect uric acid, 300 μL of OPD (10 mM), 40 μL of Fe/N-CDs, 100 μL of uricase (1 U/mL), and 100 μL of sample or standard solution contain uric acid were added into 460 μL of PB buffer (10 mM, pH = 7.4). The following experimental procedures are similar to these for detecting H_2O_2.

2.4. Determination of xanthine and uric acid in real samples

Three human serum samples and three human urine samples from individual healthy volunteers were provided by the First Hospital of Jilin University (Changchun, China). Each of these samples was examined by HPLC methods [27]. All the serum samples were diluted 10-fold with PB buffer (10 mM, pH = 7.4) prior to detecting xanthine or uric acid, and all the urine samples were respectively diluted 10-fold or 100-fold with PB buffer (10 mM, pH = 7.4) prior to detecting xanthine or uric acid. The spiked serum and urine samples were prepared by adding xanthine or uric acid standard solutions into the real samples. The procedures for detection of the real or spiked samples were similar to these described in Section 2.3.

3. Results and discussion

3.1. Characterization of Fe/N-CDs

As displayed in the image and the size statistics of particles obtained by transmission electron microscopy (TEM, Fig. 1A), the Fe/N-CDs are spherical and exhibit a good dispersibility with an average diameter of 2.3 nm.

Identification of surface chemical groups and elemental analysis of Fe/N-CDs were performed by Fourier transform infrared spectroscopy (FT-IR, Fig. 1B) and X-ray photoelectron spectroscopy (XPS, Fig. 2). In FT-IR spectrum, the broad absorption band at 3430 cm^{-1} is associated with O—H and N—H stretching vibrations, the band at 2357 cm^{-1} is assigned to the O═C═O group, the band at 1628 cm^{-1} corresponds to the stretching vibrations of C═O or C═N groups, the band at 1389 cm^{-1} originates from the bending vibrations of C—N [28,29]. The XPS spectra (Fig. 2) furtherly reveal the elemental composition of Fe/N-CDs. Three main peaks emerged at 284.5 eV, 399.2 eV, and 531.1 eV in the full scan survey spec-

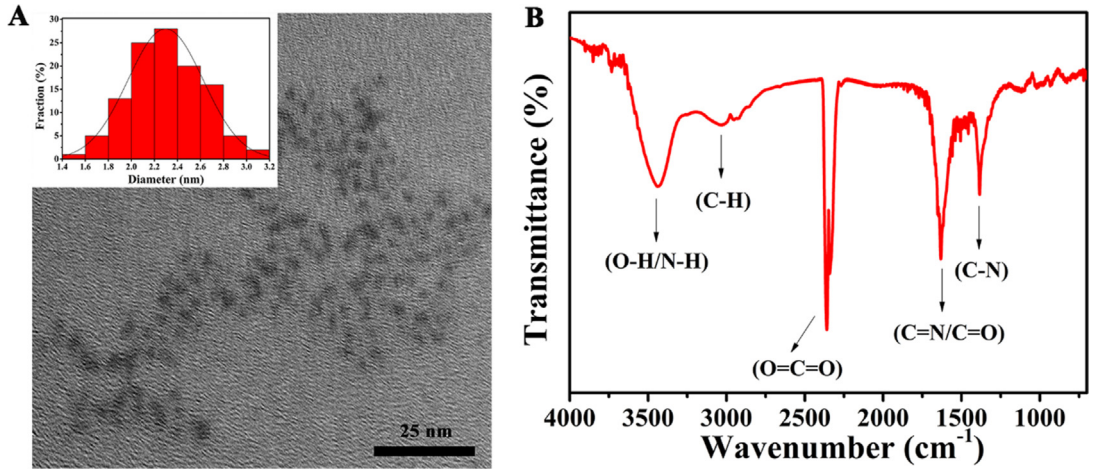

Fig. 1. (A) TEM image and particle size distribution of Fe/N-CDs. (B) FT-IR spectrum of Fe/N-CDs.

trum (Fig. 2A) of Fe/N-CDs indicate the types and ratios of dominant elements including carbon (C 1s, 56.55%), nitrogen (N1s, 7.3%), and oxygen (O 1s, 34.35%), respectively [30]. Iron also contributes a little signal at 710.8 eV in the above spectrum (Fe 2p, 1.8%). In the high-resolution spectra of C 1s (Fig. 2B), there are three peaks appeared at 284.5 eV, 285.6 eV, and 288.0 eV, which are respectively derived from C—C/C=C, C—N, and C=N/C=O groups [31]. The spectrum of N 1s (Fig. 2C) can be subdivided into three peaks at 399.3 eV, 400.0 eV, and 401.2 eV, which are ascribed to C—N—C, C—N, and N—H [23,32]. The spectrum of O 1s (Fig. 2D) is attributed to three contributions, corresponding to 530.7 eV for C—O, 531.8 eV for C=O, 532.4 eV for C—O—C/C—OH, respectively. The spectrum of Fe 2p (Fig. 2E) can be subdivided into two peaks at 710.8 and 723.7 eV, which are ascribed to Fe $2p_{3/2}$ and Fe $2p_{1/2}$ [33]. Results of XPS analysis are consistent with that obtained by FT-IR measurement.

3.2. Optical properties of Fe/N-CDs

Optical properties of Fe/N-CDs were studied by ultraviolet–visible absorption spectroscopy (UV–Vis) and fluorescence spectroscopy. As displayed in Fig. 3A, the Fe/N-CDs exhibits a broad absorption band at 200–400 nm (black line), and shows a maximum fluorescence emission at 436 nm (blue line) and a maximum fluorescence excitation at 362 nm (red line). Three excitation peaks displayed at 245 nm, 270 nm and 362 nm indicate the various excitation energy trapped on the Fe/N-CDs (red line). Fig. 3B shows the fluorescent emission spectra of the Fe/N-CDs at different excitation wavelengths between 350 nm and 410 nm, demonstrating the excitation-dependent behavior of the Fe/N-CDs, which probably originating from the surface state defects [34]. The quantum yield (QY) of the Fe/N-CDs was measured to be 9.07% by an absolute method.

3.3. Peroxidase-like activity of Fe/N-CDs

According to reported literatures [21], it is the iron element doped into CDs that gives the Fe/N-CDs intrinsic peroxidase-like catalytic activities. By using TMB and H_2O_2 as substrates, influence of the environmental pH and temperature on the peroxidase-like catalytic activities of the Fe/N-CDs (Fig. S1), and the steady-state catalytic kinetics of the Fe/N-CDs (Fig. S2) were investigated. It can be observed that the catalytic activity of the Fe/N-CDs was pH-dependent. The catalytic activities of the Fe/N-CDs were improved under acidic conditions because the low-pH environment facilitates the Fenton reaction induced by the iron element dopped in CDs, which is in accordance to the previous research reports of similar iron-doped nanoenzymes [35,36]. The testing results were fitted by the basic Michaelis-Menten equation and its double reciprocal formats to obtain the catalytic constants (Table S1). The K_m values of Fe/N-CDs with H_2O_2 and TMB were calculated as 1.297 mM and 0.736 mM, respectively.

3.4. Fluorescence emission stability of Fe/N-CDs

Effects of environmental pH and ionic strength on the spectral stability of Fe/N-CDs were explored. As depicted in Fig. S3A, fluorescence emission of Fe/N-CDs was influenced slightly by the environmental pH levels varying from 3.0 to 10.0. Fig. S3B shows that high ionic strength (NaCl, 5 M) exhibits little effect on the fluorescence emission of Fe/N-CDs. Results of photobleaching experiment (Fig. S3C) reveal the good photobleaching resistance of Fe/N-CDs under ultraviolet irradiation at 370 nm for 60 min. These results indicate the sufficient spectral stability of the synthesized Fe/N-CDs for further chemical or biological applications.

3.5. Optimization of experimental parameters

Effects of experimental conditions including amount of OPD and incubation time were investigated (Fig. S4). The optimized amount of OPD and of the incubation time prior to analysis were respectively selected as 3 mM and 30 min for the Fe/N-CDs-catalyzed oxidation. The excitation wavelength of this sensing platform was set at 370 nm for ensuring the fluorescence emission efficiencies of both Fe/N-CDs and oxOPD. The environment pH level for this sensing platform was set at 7.4 since it is the normal value of blood pH level in human body.

Experimental conditions for the detection of xanthine and uric acid were optimized in detail. Results revealed that the optimized amount of xanthine oxidase and uricase were 0.5 U/mL (Fig. S5A) and 0.1 U/mL (Fig. S6A), respectively, and a total incubation time of 30 min prior to analysis of xanthine or uric acid (Fig. S5B, S6B) was sufficient for both the enzyme-catalyzed hydrolysis and the Fe/N-CDs-catalyzed oxidation.

3.6. Sensing mechanism

The response mechanism of this sensing platform was studied by fluorescence emission spectroscopy, UV–Vis absorption spectroscopy and fluorescence decay profile (Fig. 4). One of the

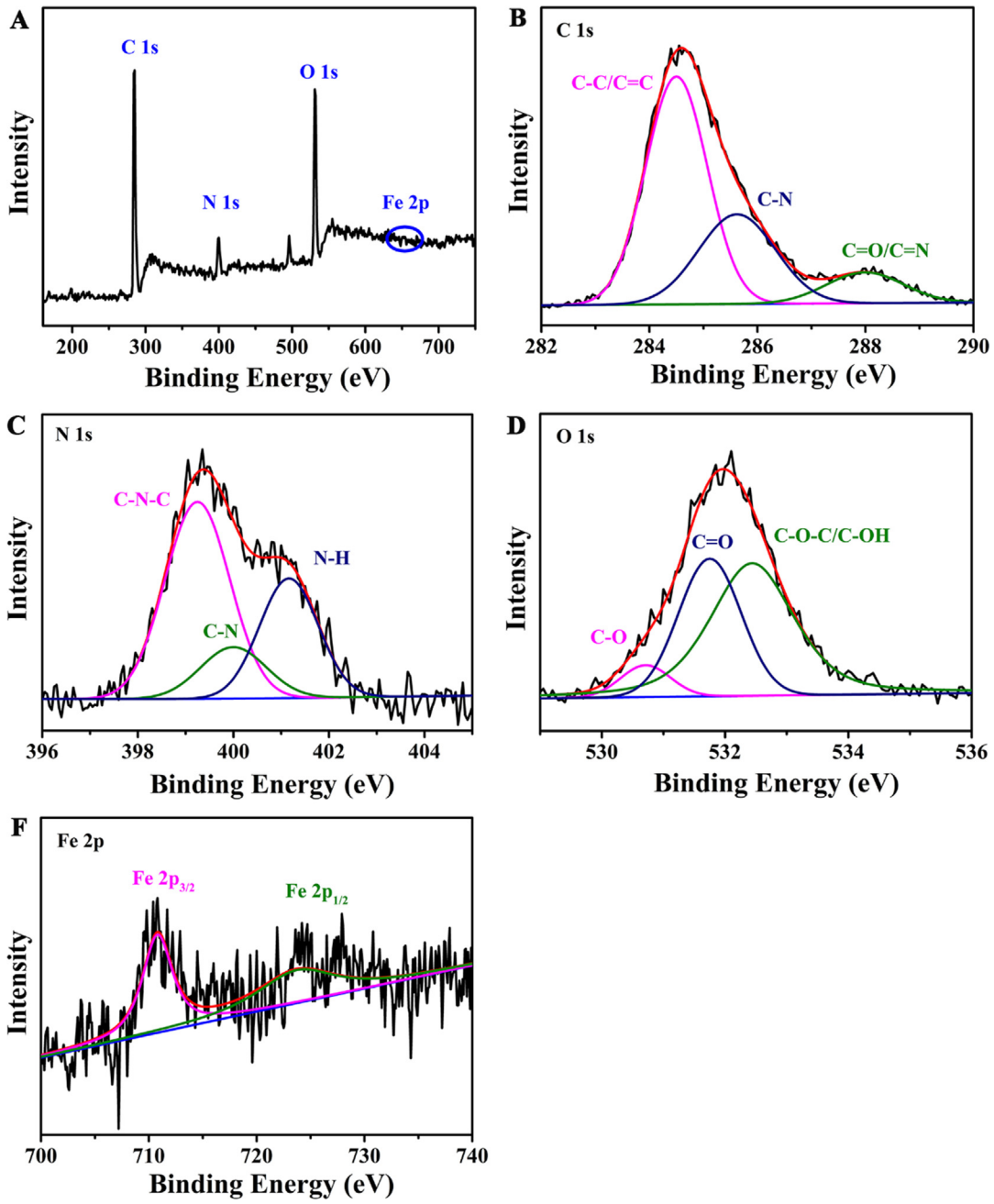

Fig. 2. XPS spectra of Fe/N-CDs. (A) Full scan survey spectrum. (B-E) High-resolution spectra of C 1s, O 1s, N 1s, and Fe 2p, respectively.

peroxidase-like properties of Fe/N-CDs is reflected in its ability to catalyze the oxidation of chromogenic substrates in the presence of H_2O_2. Spectra illustrated in Fig. 4A proved that Fe/N-CDs possess the ability for catalyzing the oxidation of TMB. As represented in Fig. 4B, the fluorescence emission of Fe/N-CDs was influenced very slightly by individually adding H_2O_2 or OPD into the testing system. However, after both H_2O_2 and OPD were added into the testing system, the fluorescence emission of Fe/N-CDs decreased significantly and a new fluorescence emission peak at 555 nm emerged, indicating the generating of oxOPD by the Fe/N-CDs-catalyzed oxidation of OPD. The oxidation product oxOPD also exhibits an absorption band at 420 nm (Fig. 4C).

It can be observed that the absorption spectrum of oxOPD (Fig. 4C) overlapped with the fluorescence emission spectrum of Fe/N-CDs (Fig. 4B). Moreover, the fluorescence lifetime of Fe/N-CDs decreased obviously after introducing H_2O_2 and OPD into the testing system. Zeta potential analyses (Fig. S7) revealed the potential values of Fe/N-CDs in absence and presence of oxOPD were −4.05 and + 7.89 mV, respectively, indicating oxOPD molecules can be bonded on the surface of Fe/N-CDs via electrostatic interaction. Therefore, Förster resonance energy transfer (FRET) from Fe/N-CDs to oxOPD was confirmed as one of the fluorescence response mechanisms of this sensing platform, which was also proved by the previous research work [37].

Under the specific catalysis of xanthine oxidase or uricase, H_2O_2 can be generated during the hydrolysis of xanthine or uric acid. Therefore, the sensitive detection of H_2O_2, xanthine and uric acid (Scheme 1) can be performed by monitoring the intensity ratio of fluorescence emission at 555 nm against that at 449 nm (F_{555}/F_{449}) or the absorbance at 420 nm (A_{420}). By changing correspond-

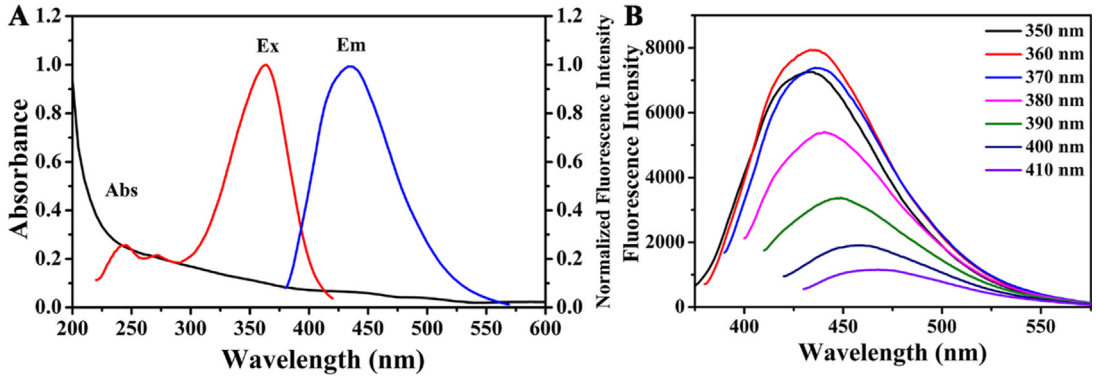

Fig. 3. (A) UV–Vis absorption (Abs), fluorescence excitation (Ex) and emission (Em) spectra of Fe/N-CDs. (B) Fluorescence emission spectra of Fe/N-CDs at various excitation wavelengths.

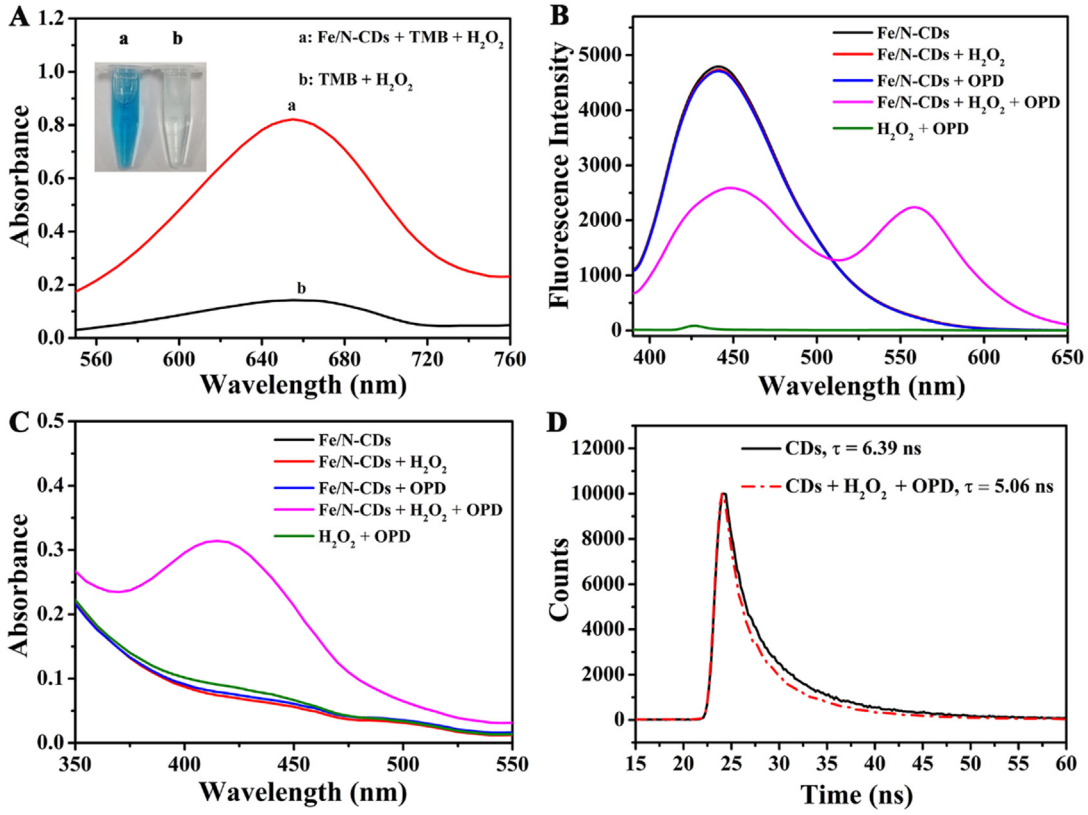

Fig. 4. (A) UV–Vis absorption spectra of testing systems containing TMB and H_2O_2 in presence and absence of catalytic Fe/N-CDs. Inset is the photograph of the corresponding testing systems. (B) Fluorescence emission and (C) UV–Vis absorption spectra of testing systems containing various reagents of the developed sensing platform. (D) Fluorescence emission decay curves of Fe/N-CDs in absence and presence of H_2O_2 and OPD. Concentration of H_2O_2 and OPD were 400 μM and 3 mM, respectively. Environmental pH level was 7.4. Fluorescence excitation wavelength was 370 nm.

ing enzymes, the sensing platform developed in this work can be furtherly employed to detect other H_2O_2 metabolism-involved metabolites.

3.7. Selectivity

To evaluate the selectivity of the present sensing platform towards xanthine and uric acid, the influence of ions and biological substances commonly coexisting in human serum or urine on the detecting results were investigated. Results illustrated in Fig. S8 reveal that no obvious interference from the above ions or substances were observed, indicating the excellent selectivity of the sensing platform.

3.8. Analytical performance

Fig. 5 demonstrates the fluorescence and UV–Vis responses of the sensing platform towards H_2O_2. Moreover, the color of the testing system changes gradually from blue to yellow under the illumination of a 365-nm UV lamp (Inset of Fig. 5A), and from colorless to yellow under daylight (Inset of Fig. 5C) along with the increasing initial concentration of H_2O_2. As shown in Fig. 5B, a good linear relationship was found between the fluorescence intensity ratio F_{555}/F_{449} and the H_2O_2 concentration ranging from 0.2 μM to 200 μM. The limit of detection (LOD) for H_2O_2 obtained by the ratiometric fluorescence mode was calculated as 0.07 μM (S/N = 3). The absorbance at 420 nm is also linear to the H_2O_2 concen-

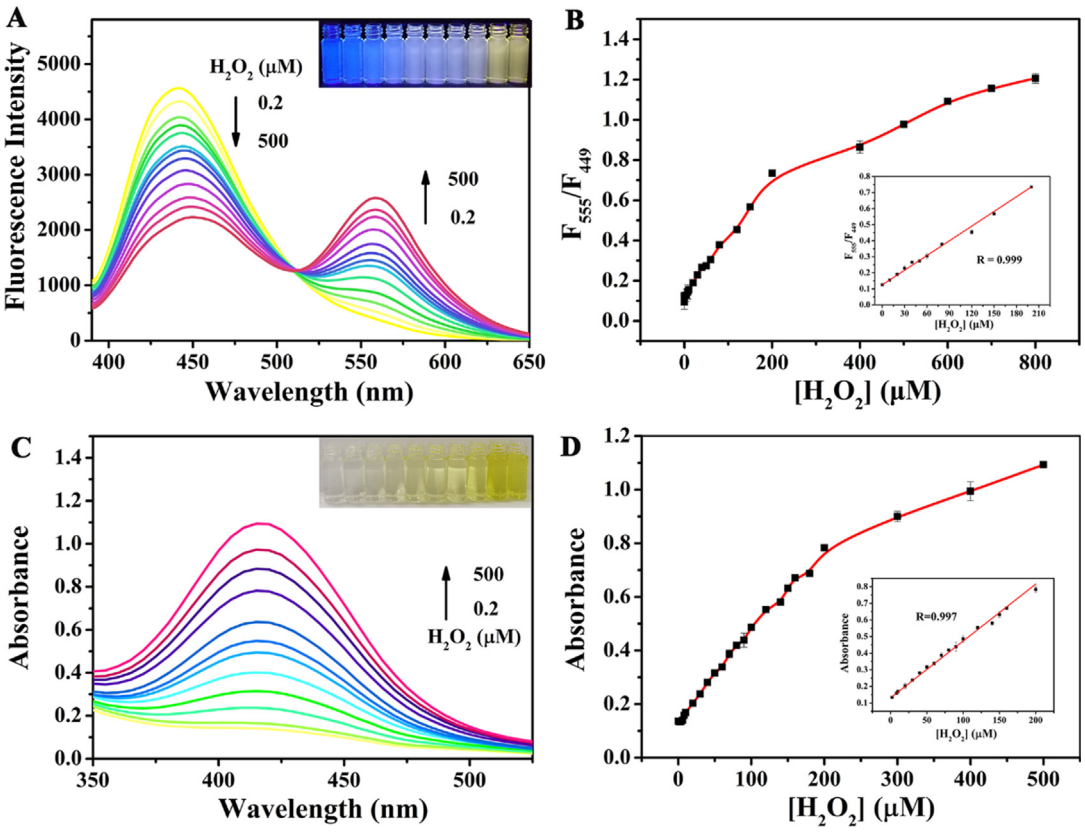

Fig. 5. (A) Fluorescence spectra of the sensing system with different initial H_2O_2 concentrations. Inset photograph shows the corresponding color changes under the illumination of a 365-nm UV lamp. (B) Plot of fluorescence responses against concentrations of H_2O_2. (C) UV–Vis absorption spectra of the sensing system with different initial H_2O_2 concentrations. The inset photograph shows the corresponding color changes under daylight. (D) Plot of absorbances against concentrations of H_2O_2.

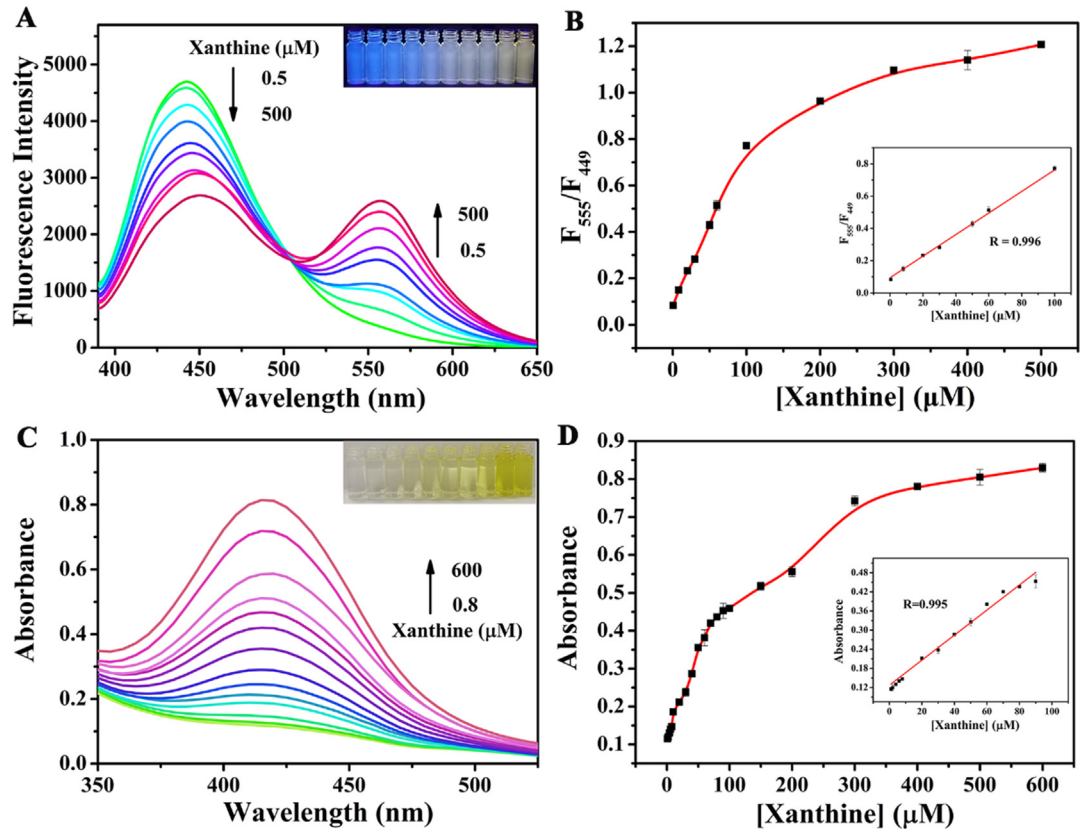

Fig. 6. (A) Fluorescence spectra of the sensing system with different initial xanthine concentrations. Inset photograph shows the corresponding color changes under the illumination of a 365-nm UV lamp. (B) Plot of fluorescence responses against concentrations of xanthine. (C) UV–Vis absorption spectra of the sensing system with different initial xanthine concentrations. The inset photograph shows the corresponding color changes under daylight. (D) Plot of absorbances against concentrations of xanthine.

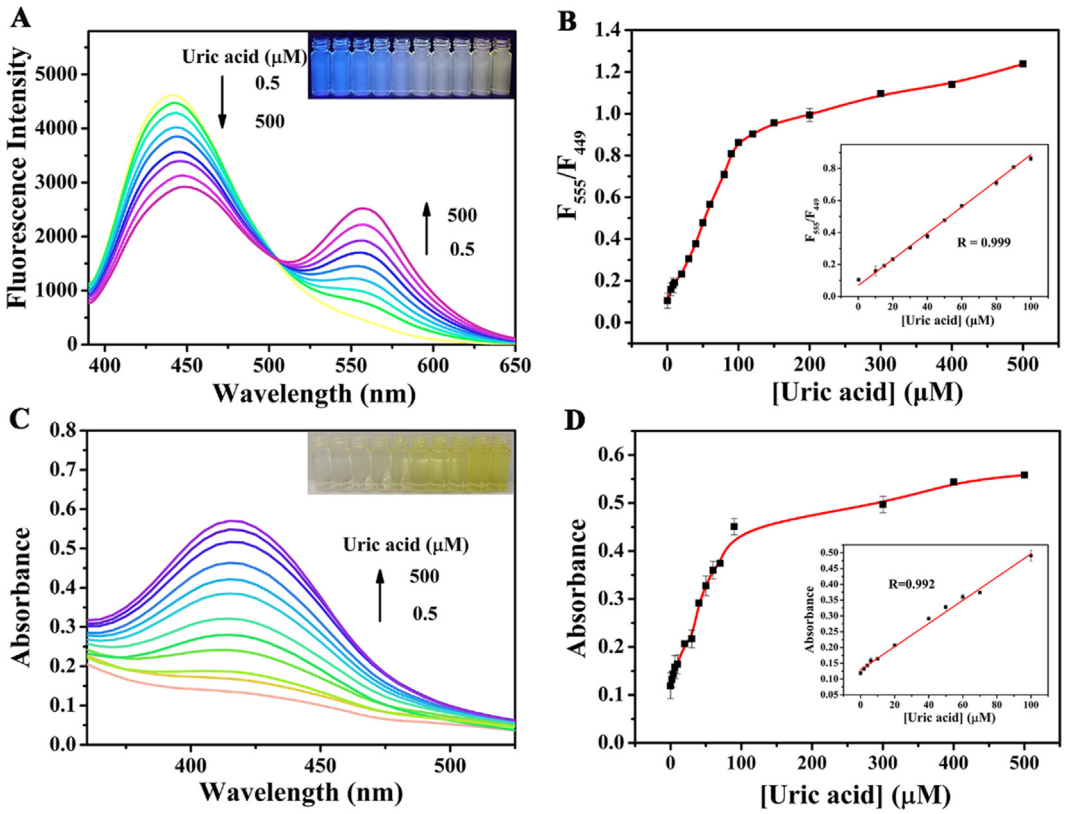

Fig. 7. (A) Fluorescence spectra of the sensing system with different initial uric acid concentrations. The inset photograph shows the corresponding color changes under the illumination of a 365-nm UV lamp. (B) Plot of fluorescence responses against concentrations of uric acid. (C) UV–Vis absorption spectra of the sensing system with different initial uric acid concentrations. The inset photograph shows the corresponding color changes under daylight. (D) Plot of absorbances against concentrations of uric acid.

Table 1
Detection results for xanthine and uric acid in real and spiked human serum and human urine samples by the proposed sensing platform and reference HPLC methods (n = 3).

Target	Testing mode	Sample	spiked	Determined (μM)	Recovery (%)	RSD (%)	HPLC method (μM)
Xanthine	Ratiometric fluorometry	Serum 1	0	4.45	–	2.6	4.57
		Serum 2	30	35.13	101.9	1.91	34.91
		Serum 3	50	54.39	99.64	0.85	54.27
		Urine 1	0	16.81	–	0.97	16.59
		Urine 2	30	47.12	101.8	1.68	46.93
		Urine 3	50	66.49	99.8	0.55	66.98
	Colorimetry	Serum 1	0	4.65	–	1.29	4.57
		Serum 2	30	33.75	97.3	3.13	34.91
		Serum 3	50	54.03	98.9	1.15	54.27
		Urine 1	0	16.24	–	2.61	16.59
		Urine 2	30	45.91	97.7	2.42	46.93
		Urine 3	50	66.44	99.7	0.38	66.98
Uric acid	Ratiometric fluorometry	Serum 1	0	25.87	–	3.91	26.93
		Serum 2	20	47.12	100.9	0.95	46.71
		Serum 3	40	65.77	97.1	2.72	65.36
		Urine 1	0	10.67	–	1.19	10.43
		Urine 1	20	30.26	99.2	0.94	30.88
		Urine 1	40	49.68	98.1	1.84	50.35
	Colorimetry	Serum 1	0	26.79	–	0.88	26.93
		Serum 2	20	46.85	99.6	0.57	46.71
		Serum 3	40	66.19	98.2	0.9	65.36
		Urine 1	0	10.24	–	1.75	10.43
		Urine 2	20	30.94	102.6	2.32	30.88
		Urine 3	40	49.69	98.2	1.57	50.35

tration in the range of 0.2–200 μM (Fig. 5D). The LOD for H_2O_2 obtained by the colorimetric (UV–Vis absorption) mode is 0.12 μM.

Similarly, the fluorescence and UV–Vis responses of the sensing platform towards xanthine and uric acid were shown in Fig. 6 and Fig. 7, respectively. The linear ranges for xanthine and uric acid are respectively 0.5–100 μM and 0.5–100 μM for ratiometric fluorescence mode, and 0.8–90 μM and 0.5–100 μM for colorimetric mode. The LODs (S/N = 3) for xanthine and uric acid are respectively 0.15 μM and 0.14 μM for ratiometric fluorescence mode, and 0.52 μM and 0.47 μM for colorimetric mode.

The above results indicate that the sensitivities of this sensing platform for xanthine and uric acid detection are comparable to

or slightly better than many previously reported methods (Table S2, S3).

3.9. Detection of xanthine and uric acid in real sample

To estimate the practicability of the present sensing platform for detecting xanthine and uric acid in human fluid samples, it was applied to examining the real and spiked samples by both ratiometric fluorescent and colorimetric modes. The good accordance between results obtained by this sensing platform and by reference HPLC methods (Table 1) indicates the excellent practicability of this sensing platform.

4. Conclusion

In this work, a multifunctional nanomaterial Fe/N-CDs with properties of both peroxidase-like catalysis and fluorescence emission was prepared via a one-pot hydrothermal method. By utilizing the Fe/N-CDs-catalyzed oxidation of a routine chromogenic development reagent OPD in presence of H_2O_2, fluorescent oxOPD which would induce the quenching of fluorescence emitted form Fe/N-CDs via FRET process was generated. The intensity ratio of fluorescence emitted by oxOPD against that emitted by Fe/N-CDs, as well as the absorbance of oxOPD indicated the amount of H_2O_2 consumed during the above oxidation reaction, therefore they were employed as the response signals for realizing the ratiometric fluorescence and the colorimetric detections of H_2O_2. Since H_2O_2 would be generated by corresponding enzyme-catalyzed hydrolysis reactions of various metabolites in human fluid, determination of these metabolites was realized based on the above method for detecting H_2O_2. Finally, a universal sensing platform for sensitive detecting metabolites involved in H_2O_2 metabolism in human fluid was established. This sensing platform exhibits high accuracy, selectivity and sensitivity for determination of xanthine and uric acid in real human serum and urine samples, demonstrating its promising potential for future applications in study of clinical diagnosis.

5. Compliance with ethical standards

All applicable international, national, and/or institutional guidelines for the collection and use of human serum and urine samples were followed.

CRediT authorship contribution statement

Wei Zhang: Conceptualization, Methodology, Software, Investigation, Validation, Data curation, Writing – original draft. **Yanhua Wu:** . **Xin Liu:** Data curation. **Yibing Liu:** Data curation. **Yue Zhang:** Software. **Wei Wang:** Validation. **Xiaowei Mu:** Writing – review & editing. **Rui Su:** Software. **Ying Sun:** . **Daqian Song:** Supervision. **Xinghua Wang:** Writing – review & editing.

Declaration of Competing Interest

The authors declare that they have no known competing financial interests or personal relationships that could have appeared to influence the work reported in this paper.

Acknowledgments

This work was supported by the Fundamental Research Funds for the Central Universities of China, the Research Project of Education Department of Jilin Province (No. JJKH20200944KJ and No. JJKH20211187KJ), and the Training Program of Excellent Young Teachers of Jilin University.

Appendix A. Supplementary material

Supplementary data to this article can be found online at https://doi.org/10.1016/j.saa.2022.121003.

References

[1] S. Chen, X. Hai, X.-W. Chen, J.-H. Wang, In situ growth of silver nanoparticles on graphene quantum dots for ultrasensitive colorimetric detection of H_2O_2 and glucose, Anal. Chem. 86 (13) (2014) 6689–6694.
[2] N. Li, A. Than, X. Wang, S. Xu, L. Sun, H. Duan, C. Xu, P. Chen, Ultrasensitive profiling of metabolites using tyramine-functionalized graphene quantum dots, ACS Nano. 10 (3) (2016) 3622–3629.
[3] Y. Zhang, N. Feng, S. Zhou, X. Xin, Fluorescent nanocomposites based on gold nanoclusters for metal ion detection and white light emitting diodes, Nanoscale. 13 (7) (2021) 4140–4150.
[4] X.-X. Wang, Q.i. Wu, Z. Shan, Q.-M. Huang, BSA-stabilized Au clusters as peroxidase mimetics for use in xanthine detection, Biosens. Bioelectron. 26 (8) (2011) 3614–3619.
[5] S.-H. Huang, Y.-C. Shih, C.-Y. Wu, C.-J. Yuan, Y.-S. Yang, Y.-K. Li, T.-K. Wu, Detection of serum uric acid using the optical polymeric enzyme biochip system, Biosens. Bioelectron. 19 (12) (2004) 1627–1633.
[6] Y. Liu, H. Li, B. Guo, L. Wei, B.o. Chen, Y. Zhang, Gold nanoclusters as switch-off fluorescent probe for detection of uric acid based on the inner filter effect of hydrogen peroxide-mediated enlargement of gold nanoparticles, Biosens. Bioelectron. 91 (2017) 734–740.
[7] R.J. Johnson, D.-H. Kang, D. Feig, S. Kivlighn, J. Kanellis, S. Watanabe, K.R. Tuttle, B. Rodriguez-Iturbe, J. Herrera-Acosta, M. Mazzali, Is there a pathogenetic role for uric acid in hypertension and cardiovascular and renal disease?, Hypertension 41 (6) (2003) 1183–1190
[8] S. Srinivasan, P. Kalaiselvi, R. Sakthivel, V. Pragasam, V. Muthu, P. Varalakshmi, Uric acid: an abettor or protector in calcium oxalate urolithiasis? Biochemical study in stone formers, Clin. Chim. Acta. 353 (2005) 45–51.
[9] I. Baranowska, M. Zydroń, Quantitative structure-retention relationships of xanthines in RP HPLC systems with the new Chromolith RP-18e stationary phases, Anal. Bioanal. Chem. 373 (8) (2002) 889–892.
[10] M. Elham, A. Jafar, H. Javad, Rhodamine B chemiluminescence improved by mimetic AuCu alloy nanoclusters and ultrasensitive measurement of H_2O_2 glucose and xanthine, Anal. Sci. 35 (2019) 35.
[11] L.A. Mercante, M.H.M. Facure, R.C. Sanfelice, F.L. Migliorini, L.H.C. Mattoso, D.S. Correa, One-pot preparation of PEDOT:PSS-reduced graphene decorated with Au nanoparticles for enzymatic electrochemical sensing of H_2O_2, Appl. Surf. Sci. 407 (2017) 162–170.
[12] R.K. Bera, A. Anoop, C.R. Raj, Enzyme-free colorimetric assay of serum uric acid, Chem. Commun. 47 (41) (2011) 11498, https://doi.org/10.1039/c1cc13349g.
[13] N.E. Azmi, N.I. Ramli, J. Abdullah, M.A. Abdul Hamid, H. Sidek, S. Abd Rahman, N. Ariffin, N.A. Yusof, A simple and sensitive fluorescence based biosensor for the determination of uric acid using H_2O_2-sensitive quantum dots/dual enzymes, Biosens. Bioelectron. 67 (2015) 129–133.
[14] T.K. Behera, S.C. Sahu, B. Satpati, B. Bag, K. Sanjay, B.K. Jena, Branched platinum nanostructures on reduced graphene: an excellent transducer for nonenzymatic sensing of hydrogen peroxide and biosensing of xanthine, Electrochimica Acta. 206 (2016) 238–245.
[15] S. Li, L. Wang, X. Zhang, H. Chai, Y. Huang, A. Co, N co-doped hierarchically porous carbon hybrid as a highly efficient oxidase mimetic for glutathione detection, Sens. Actuat. B 264 (2018) 312–319.
[16] X. Wang, L.i. Qin, M. Lin, H. Xing, H. Wei, Fluorescent graphitic carbon nitride-based nanozymes with peroxidase-like activities for ratiometric biosensing, Anal. Chem. 91 (16) (2019) 10648–10656.
[17] Y. Xia, K. Sun, Y.-N. Zuo, S. Zhu, X.-E. Zhao, Fluorescent MOF-based nanozymes for discrimination of phenylenediamine isomers and ratiometric sensing of o-phenylenediamine, Chinese Chem. Lett. 08 (2021) 083.
[18] D. Yang, Q. Li, S.K. Tammina, Z. Gao, Y. Yang, Cu-CDs/H_2O_2 system with peroxidase-like activities at neutral pH for the co-catalytic oxidation of o-phenylenediamine and inhibition of catalytic activity by Cr(III), Sens. Actuat. B 319 (2020) 128273.
[19] L. Lin, Y. Xiao, Y. Wang, Y. Zeng, Z. Lin, X. Chen, Hydrothermal synthesis of nitrogen and copper co-doped carbon dots with intrinsic peroxidase-like activity for colorimetric discrimination of phenylenediamine isomers, Mikrochim. Acta 186 (2019) 288.
[20] D. Mathivanan, S.K. Tammina, X. Wang, Y. Yang, Dual emission carbon dots as enzyme mimics and fluorescent probes for the determination of o-phenylenediamine and hydrogen peroxide, Mikrochim. Acta 187 (2020) 292.
[21] Y. Dong, J. Li, L. Shi, Z. Guo, Iron impurities as the active sites for peroxidase-like catalytic reaction on graphene and its derivatives, ACS Appl. Mater. Inter. 7 (28) (2015) 15403–15413.
[22] C. Lu, Y. Liu, Q. Wen, Y. Liu, Y. Wang, H. Rao, Z. Shan, W. Zhang, X. Wang, Ratiometric fluorescence assay for L-Cysteine based on Fe-doped carbon dot nanozymes, Nanotechnology 31 (2020) 445703.

[23] W. Yang, TingTing Huang, M. Zhao, F. Luo, W. Weng, Q. Wei, Z. Lin, G. Chen, High peroxidase-like activity of iron and nitrogen co-doped carbon dots and its application in immunosorbent assay, Talanta 164 (2017) 1–6.
[24] L. Wang, Y. Liu, Z. Yang, Y. Wang, H. Rao, G. Yue, C. Wu, C. Lu, X. Wang, A ratiometric fluorescence and colorimetric dual-mode assay for H2O2 and xanthine based on Fe, N co-doped carbon dots, Dyes Pigments. 180 (2020) 108486.
[25] N.a. Xiao, S.G. Liu, S. Mo, Y.Z. Yang, L. Han, Y.J. Ju, N.B. Li, H.Q. Luo, B, N-carbon dots-based ratiometric fluorescent and colorimetric dual-readout sensor for $_{H}2_{O}2$ and $_{H}2_{O}2$-involved metabolites detection using $ZnF_{e}2_{O}4$ magnetic microspheres as peroxidase mimics, Sens. Actuat. B 273 (2018) 1735–1743.
[26] D. Zhu, S. Zhuo, C. Zhu, P. Zhang, W. Shen, Synthesis of catalytically active peroxidase-like Fe-doped carbon dots and application in ratiometric fluorescence detection of hydrogen peroxide and glucose, Anal. Methods 11 (20) (2019) 2663–2668.
[27] Y.u. Wang, M. Deng, B. Deng, L. Ye, X. Fei, Z. Huang, Study on the diagnosis of gout with xanthine and hypoxanthine, J. Clin. Lab. Anal. 33 (5) (2019), https://doi.org/10.1002/jcla.2019.33.issue-510.1002/jcla.22868.
[28] S. Liu, J. Cui, J. Huang, B. Tian, F. Jia, Z. Wang, Facile one-pot synthesis of highly fluorescent nitrogen-doped carbon dots by mild hydrothermal method and their applications in detection of Cr(VI) ions, Spectrochim. Acta A 206 (2019) 65–71.
[29] Z. Han, D. Nan, H. Yang, Q. Sun, S. Pan, H. Liu, X. Hu, Carbon quantum dots based ratiometric fluorescence probe for sensitive and selective detection of Cu^{2+} and glutathione, Sens. Actuat. B 298 (2019) 126842.
[30] S. Liu, J. Tian, L. Wang, Y. Zhang, X. Qin, Y. Luo, A.M. Asiri, A.O. Al-Youbi, X. Sun, Hydrothermal treatment of grass: a low-cost, green route to nitrogen-doped, carbon-rich, photoluminescent polymer nanodots as an effective fluorescent sensing platform for label-free detection of Cu(II) ions, Adv. Mater. 24 (2012) 2037–2041.
[31] X.-X. Zou, G.-D. Li, Y.-N. Wang, J. Zhao, C. Yan, M.-Y. Guo, L.u. Li, J.-S. Chen, Direct conversion of urea into graphitic carbon nitride over mesoporous TiO_2 spheres under mild condition, Chem. Commun. 47 (3) (2011) 1066–1068.
[32] Y. Li, Y. Weng, S. Lu, M. Xue, B. Yao, W. Weng, T. Zheng, One-step hydrothermal synthesis of N, Fe-codoped carbon dots as mimic peroxidase and application on hydrogen peroxide and glucose detection, J. Nanomate. 2020 (2020) 1–11.
[33] X. Tian, J. Luo, H. Nan, Z. Fu, J. Zeng, S. Liao, Binary transition metal nitrides with enhanced activity and durability for the oxygen reduction reaction, J. Mater. Chem. A 3 (32) (2015) 16801–16809.
[34] Y.Z. Fan, Y. Zhang, N.a. Li, S.G. Liu, T. Liu, N.B. Li, H.Q. Luo, A facile synthesis of water-soluble carbon dots as a label-free fluorescent probe for rapid, selective and sensitive detection of picric acid, Sens. Actuat. B 240 (2017) 949–955.
[35] X. Xie, Y. Wang, X. Zhou, J. Chen, M. Wang, X. Su, Fe-N-C single-atom nanozymes with peroxidase-like activity for the detection of alkaline phosphatase, Analyst 146 (3) (2021) 896–903.
[36] X. Zhou, M. Wang, X. Su, Sensitive glutathione S-transferase assay based on Fe-doped hollow carbon nanospheres with oxidase-like activity, Sens. Actuat. B 338 (2021) 129777.
[37] D. Su, X. Han, X.u. Yan, R. Jin, H. Li, D. Kong, H. Gao, F. Liu, P. Sun, G. Lu, Smartphone-assisted robust sensing platform for on-site quantitation of 2,4-dichlorophenoxyacetic acid using red emissive carbon dots, Anal. Chem. 92 (18) (2020) 12716–12724.